Surface Review and Letters, Vol. 11, Nos. 4 & 5 (2004) 391–401

World Scientific
www.worldscientific.com

CHARACTERIZATION OF Al^+ SECONDARY ION EMISSION PRODUCED BY Ne^+ AND Ar^+ BOMBARDMENT OF ALUMINIUM SURFACE

A. TOLSTOGOUZOV*
Department of Chemistry, University of Florence,
Via della Lastruccia 3, 50019 Sesto Fiorentiono (Fi), Italy
alexander.tolstoguzov@unifi.it

S. F. BELYKH
Department of Chemistry, University of Antwerp (UIA),
Antwerp (Wilrijk) B-2610, Belgium

M. STEPANOVA and S. K. DEW
Department of Electrical and Computer Engineering,
University of Alberta, Edmonton, Alberta T6G 2V4, Canada

C. PAGURA
Istituto per l'Energetica e le Interfasi (CNR IENI),
Corso Stati Uniti 4, Padua 35127, Italy

Received 21 June 2004

This paper reports the characterization of the velocity (energy) dependencies of the Al^+ secondary ion emission produced by 0.5 keV and 5 keV Ne^+ and Ar^+ bombardment of polycrystalline pure aluminium. The distributions of secondary Al^+ ions over their kinetic energy were measured for emission energies of 1–1000 eV without applying electric fields to force the ions into the mass–energy analyzer. To extract the ionization probability, the measured energy distributions of emitted ions were normalized with respect to reference energy distributions of neutral atoms. The reference distributions were obtained by original numerical simulations, as well as analytically, through a sophisticated normalization of the Thompson distribution. It was shown that for both extraction methods, the logarithmic plots of the normalized secondary ion fraction versus the normal component of the reciprocal ion velocity (the reciprocal or inverse velocity plots) are nonmonotonic, with two peaks and two linear portions situated at a low emission energy (E_k = 5–25 eV) and at a high emission energy (E_k = 80–280 eV). The linear portions were fit by exponential dependency $P^+ \propto \exp(-v_0/v_n)$ with two different values of the characteristic velocity v_0. For the low emission energy, the value $v_{01} \sim (3.3 \pm 0.2) \times 10^6$ cm/s was independent of the mass and energy of the projectiles. However, for the high emission energy, the characteristic velocity depended on the projectile's mass, M, namely $v_{02} \sim (5.3 \pm 0.3) \times 10^6$ cm/s for Ne^+ and $v_{02} \sim (8.1 \pm 0.3) \times 10^6$ cm/s for Ar^+; the ratio $v_{02}(Ne^+)/v_{02}(Ar^+)$ is close to the value $\sqrt{\mathbf{M}_{Ne}/\mathbf{M}_{Ar}}$. This indicates that ballistic mechanisms might contribute to affect the high-energy part of the reciprocal velocity plots along with nonballistic ionization processes, which are generally believed to be the only significant factor for the plots.

Keywords: Aluminium; computer simulations; ion emission; ion–solid interactions; secondary ion mass spectrometry.

*Corresponding author. Fax: +39 055 457 3120. Tel: +39 055 457 3116.

1. Introduction

Numerous models have been proposed to explain the mechanism(s) of secondary ion formation under ion beam bombardment. (For a review, see Refs. 1–4 and references cited therein.) The key parameter in all the models is the dependence of the ionization probability P^+ on the velocity of emitted ions. The tunneling, bond-breaking, and combined models[1–7] suppose that ionization basically occurs via electron exchange between a localized valence level (or more properly, a narrow band) of the emitted atom and electronic states in the conduction band of a solid. Such models predict a strong velocity dependence described by the Hagstrum's exponential law[8]

$$P^+ \propto \exp(-v_0/v_n)\,, \tag{1}$$

where v_n is the normal component of the velocity of the emitted ion, and v_0 is the characteristic velocity (ionization parameter) depending on the ion species and on peculiar properties of ion–solid interactions. The nonequilibrium thermodynamic models[1,9] describe the secondary ion emission in terms of the "local electronic temperature," which increases under atomic collisions in the target. This approach results in a much weaker power-law–velocity dependence, and it remains a contentious issue in the literature.[10] All the theories consider sputtering and ionization as independent processes, although the validity of such a partition has never been confirmed experimentally.

For the k-isotope of the i-component of the target, the detected signal S of singly-charged positive atomic secondary ions is represented by

$$\begin{aligned} {}^kS_i(E,\,\Omega) = I \cdot {}^kN_i(E,\,\Omega) \cdot {}^kP_i^+(E,\,\Omega) \\ \cdot {}^kT_i(E,\,\Omega) \cdot {}^k\gamma_i \cdot C_i\,, \end{aligned} \tag{2}$$

where I is the ion beam current through the sample area "seen" by the detector, N is the normalized energy distribution of neutral sputtered atoms, P^+ is the ionization probability, T is an apparatus factor including the analyzer transmission and the detector efficiency, γ is the isotope abundance, C is the relative atomic concentration, E and Ω define the kinetic energy and direction of particles emitted, and the superscript k indicates the mass of the isotope. Thus, if the values I, N, T, and C are known, the ionization probability P^+ can be extracted from the measured signal S.

To date, numerous attempts have been made to extract information on ionization mechanisms from the kinetic energy distributions (EDs) of the secondary ions (Refs. 4, 11–16, to name but a few.) However, precise ED measurements complemented with a rigorous extraction procedure still remain a challenge. In particular, the measurement of energy distributions is a complicated task and subject to severe apparatus artefacts. Thus, the systems that use electric fields to force the ions into the mass–energy analyzer — i.e. practically all standard secondary ion mass spectrometers — introduce distortions in the dependencies $S(E,\,\Omega)$ which are difficult to eliminate or to take a proper account of. We address the reader to Wittmaack's papers,[2,17] where he criticizes the infinite velocity method[14,15,18] for details.

Another challenge is related to the evaluation of the energy distribution of neutral sputtered atoms $N(E,\,\Omega)$. In principle, $N(E,\,\Omega)$ can be measured directly using post-ionization techniques.[19–22] However, such measurements are complex and rarely encountered. Alternatively, the distributions $N(E,\,\Omega)$ can be simulated numerically.[23] In many studies, $N(E,\,\Omega)$ is simply represented with the well known Thompson distribution.[24] However, the Thompson distribution has been found to be unreliable, particularly for low projectile energy, large incident angle, and light targets.[22,25] In addition, the Thompson formula needs to be properly normalized in order to extract quantitative information on ion formation processes from ED measurements. To our knowledge, neither the reliability of the Thompson formula has been investigated when applied to such an extraction, nor an appropriate normalization suggested.

The goal of the present work is to examine the velocity (energy) dependencies of the Al^+ secondary ion formation over a wide range of the emission energy E = 1–1000 eV. We used different projectiles (Ne^+ and Ar^+) with different energies (0.5 keV and 5 keV) to investigate the effect of bombardment conditions on the ion yield. To improve the accuracy of ED measurements,[2,17] our samples were set at a fixed (ground) potential without applying any extracting electric fields in the space between the sample and the analyzer. We also computed the distribution $N(E,\,\Omega)$ using an original numerical model,[26] as well as estimated it analytically with a specially normalized Thompson distribution.

From the measured EDs, we extracted the velocity dependence of the ionization probability $P^+(1/v_n)$ using both the numerical and analytical functions $N(E, \Omega)$, and compared the results in order to determine whether the Thompson distribution was fit for this purpose.

2. Experimental

We used an analytical grade polycrystalline Al (99.999%) foil manufactured by Goodfellow. The sample was initially rinsed with ethanol, and was, after introduction into the analytical chamber, thoroughly cleansed by Ar^+ sputtering for 3–5 h. Surface cleanness was monitored through secondary ion mass spectra.

Details of our dedicated system and the approach to measure the kinetic energy distributions of sputtered (and scattered) ions have been reported in our previous publications.[27–30] In brief, a monoenergetic inert gas ion beam was produced by an electron-impact ionization source IQE 12/38. The ion current I was in the range of 0.2–2 μA, depending on the mass and energy of the projectiles. The raster-scanned projectile beam was applied to a target area of about 1.5×1.5 mm^2. A 75% electronic gating of the registration system was used during the collection of mass and energy spectra. The measurements were performed using the "in-plane" geometry, and the incident angle of the projectiles was 30° with respect to the sample surface.

The secondary ions emitted at a small fixed angle ($\Delta\Omega \sim 10^{-4}$ sr) along the normal to the sample surface were mass and energy analyzed by the Hiden EQS 1000 system. The system combines a high transmission electrostatic energy analyzer with a quadrupole mass spectrometer, and operates with constant absolute energy and mass resolution. At the typical passing energy of $E_a = 80$ eV, the energy resolution ΔE_a is ca. 3.5 eV full-width at half maximum (FWHM), and the mass resolution ΔM (FWHM) is 0.75 amu. Under our particular experimental conditions, the ED measurements can be considered as angular-resolved with well defined emission angle. Therefore, we ignore any angular dependence in Eq. (2). All the elements of the EQS 1000 Probe are floated at the reference potential corresponding to the measured emission energy E, and for a given type of secondary ion, the transmission of the system is practically an energy-independent function. Our ion-trajectory calculations show that this condition holds at least true for quasi-paraxial, not-too-divergent ion beams with energies up to $E = 400$–500 eV. An electrodynamic element (the quadrupole mass analyzer) does not hamper ray tracing of the ion trajectories, since all ions pass through the quadrupole with the same constant energy E_a. The detector efficiency is approximately constant in the energy regimes considered for identical ion species of the same mass and charge, since they impinge upon the first dynode of the SEM with the same energy (velocity) independent of their emission energy. Thus, we consider the apparatus factor T in Eq. (2) as a constant parameter at the energy range mentioned above.

The operating pressure in the analytical chamber was $(3–5) \times 10^{-7}$ Pa. The residual gas atmosphere was carefully controlled by the same Hiden EQS 1000 system: partial pressure of the working gas (Ne or Ar) was at least two orders of magnitude higher than the pressures of residual gas species.

The energy distributions of Al^+ secondary ions were measured under steady-state bombardment conditions using a digital scan with a variable energy step (1–50 eV) and a dwell time (up to 10 s) dependent on the signal intensity. Final ED data were averaged over 4–6 successive measurements to improve the counting statistics. The ion intensities were corrected for dead-time losses of an ion-counting secondary electron multiplier through a procedure similar to that described in Ref. 31.

3. The Numerical Model for $N(E)$ and Normalized Thompson Formula

We computed the energy distributions of neutral sputtered atoms $N(E)$ for the given direction of emission Ω through the approach described in detail in Ref. 26. We solved numerically a set of master equations that describe cascades generated in a target by ion impact. The equations include: (i) collisions of projectiles with target atoms at rest, (ii) knockout of target atoms by the projectiles (creating primary recoils), and (iii) knockout of target atoms by recoils already set in motion (creating secondary recoils). The target was considered as semi-infinite and structureless. Only elastic

binary collisions were included. The free path length between successive collisions was fixed: $L = (\rho\sigma)^{-1}$, where ρ is the target number density and σ is the total interaction cross-section. This model of path length, first applied in Monte Carlo codes, is known as "liquid."[23] The treatment of path length characterizes the difference between the master equation used in this work and the well known Boltzmann equation.[32,33] The latter implies randomly distributed path lengths, with mean $\bar{L} = (\rho\sigma)^{-1}$. The advantages of using a fixed path length have been discussed elsewhere.[26,34] A screened Coulomb potential with the power-law screening function[26,35] was used to approximate the differential collision cross-section. To obtain a realistic dependency of the sputtering yield on the ion incident angle, as well as accurate angular distributions of sputtered atoms, the deflection of incoming projectiles and focusing of emitted particles when they passed the surface were accounted for. Both projectile deflection and recoil focusing were described by a unified few-collision approach and combined with the bulk master equation through sophisticated boundary conditions, as described in detail in Ref. 26. For emitted atoms, overcoming of a planar surface barrier was included following the well-known formalism,[36] which comprises a decrease of the atom energy by U and a change of its polar angle of emission to arccos $[(E\cos^2\theta - U)/(E-U)]^{1/2}$, where E and θ are, respectively, the energy and the polar angle of the atom before overcoming the barrier and U is the surface-binding energy.

With the exception of a few details such as the interatomic potential, the sputtering model used in this work is similar to that underlying the TRIM.SP code.[23] The major difference is that solution of master equations is representative of highly averaged behavior and not that of individual trajectories. Such an approach has an important advantage of being immune to computation statistics. In Refs. 26 and 35, angular and angle-resolved energy distributions obtained by our approach have been compared with experiments for Si, Ge, Al, and Cu, and have demonstrated good agreement. Also, simulated total sputtering yields were in reasonable agreement with experiment for 23 targets.[35]

We also evaluated the energy distributions of sputtered atoms $N(E)$ with a normalized Thompson distribution. Traditional sputtering theory[24,32] provides the well known distribution of ion-sputtered particles over their energy of emission

$$N_T(E) \propto E(E+U)^{-3+2m}\,, \tag{3}$$

which is known as the Thompson or the Sigmund–Thompson formula and m being the binary interaction parameter.[32,33] The distribution described by Eq. (3) has a characteristic maximum at $E = U/(2-2\text{ m})$ and asymptotically decreases at high emission energies. It does not depend on the bombarding energy and incident angle of the projectiles. In Refs. 26 and 35, the Thompson distributions were compared with experimental results for Cu and Al and were found to decrease somewhat too slow in the tail portion. In this paper, we are attempting to find out whether this discrepancy is critical for applications of the Thompson distribution to extract the ionization probability from the measured energy distributions of secondary ions.

To compare the Thompson distribution with experimental or simulated data, the Thompson distribution should be appropriately normalized. Conventionally, Eq. (3) is normalized to the maximum of the distribution to which it is compared. However, only distribution shapes can be compared in such a way, and not the absolute differential sputter yields. Since absolute angle-resolved differential yields were important for our work, we used another scaling of Eq. (3). For a given direction of emission Ω, we normalized the Thompson distribution to the differential yield of atoms sputtered in the direction Ω. To achieve this, we required

$$A(\Omega)\int_0^{E_{\max}(\Omega)} E(E+U)^{-3+2m}dE = Y(\Omega)\,, \tag{4}$$

where $Y(\Omega)$ is the differential yield of atoms sputtered in the direction Ω, $E_{\max}(\Omega)$ is the maximum energy of emission for the same direction, and $A(\Omega)$ is the normalization coefficient to be defined. We obtained the values $Y(\Omega)$ and $E_{\max}(\Omega)$ from our numerical simulations. For the interaction parameter m, we used the estimate $m = 0.2$, which is close to that employed in our modeling.[26,35] From Eq. (4), we defined the constant $A(\Omega)$ and used it to obtain the normalized Thompson distribution:

$$N_T(E, \Omega) = A(\Omega)E(E+U)^{-3+2m}\,. \tag{5}$$

It is noteworthy that $Y(\Omega)$ and $E_{\max}(\Omega)$ in Eq. (4) are functions of the direction of emission Ω. Although sputtering is often assumed to be isotropic in keV

ion energy regimes, the angular distributions of sputtered atoms are in fact always direction-sensitive to some extent, with the most pronounced anisotropies occurring at oblique incidence of projectiles.[26] Thus, in contrast to the conventional approach, $Y(\Omega)$ and $E_{\max}(\Omega)$ in Eq. (4) capture the direction sensitivity of sputtering. As a result, the constant A is a function of the emission direction Ω and so is the normalized Thompson distribution N_T. This feature of being direction-dependent is particularly important as far as oblique projectile incidence is concerned, when the direction sensitivity is particularly pronounced.

From the formalism (4,5), it follows that

$$\int_0^{E_{\max}(\Omega)} N_T(E,\,\Omega)dE = Y(\Omega)\,, \tag{6}$$

and

$$\iint_0^{E_{\max}(\Omega)} N_T(E,\,\Omega)dE\,d\Omega = \int Y(\Omega)d\Omega = Y_0\,, \tag{7}$$

where Y_0 is the total sputtering yield as obtained from our numerical modeling. Equations (6) and (7) demonstrate that the distribution N_T $(E,\,\Omega)$ is normalized to both the differential and the total sputtering yield. With such a normalization, the Thompson formula becomes sensitive to the bombardment geometry. The normalized Thompson formula is also dependent on the energy of bombarding ions, since the distribution $Y(\Omega)$ and the total yield Y_0 that define the factor A are functions of the ion energy.

4. Results

The experimental energy distributions of Al$^+$ secondary ions are shown in Fig. 1, and the parameters that characterize the distributions are listed in Table 1. Here, the most probable energy $E_{\rm mp}$, represents the energy at the peak of the distributions; width $\Delta E_{0.5}$, the FWHM; $E_{\rm avr}$, the average energy over the ranges E = 1–100 eV for E_0 = 0.5 keV and E = 1–1000 eV for E_0 = 5 keV. The values of all these parameters exhibit an evident increase with the increase in the projectile energy, whereas $E_{\rm mp}$ and $\Delta E_{0.5}$ are practically independent of the projectile mass, and only $E_{\rm avr}$ is somewhat larger for 5 keV Ar$^+$ than for 5 keV Ne$^+$ projectiles.

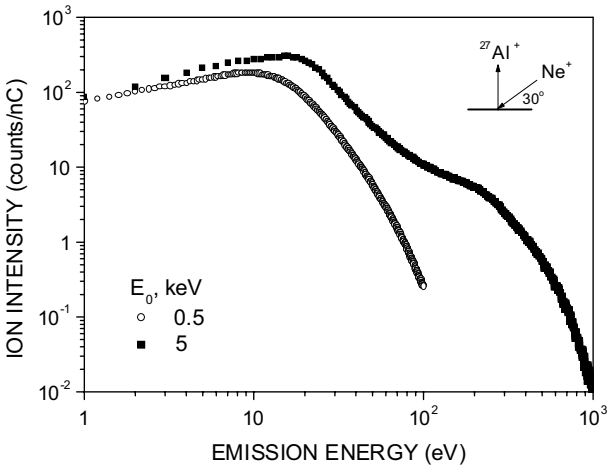

(a)

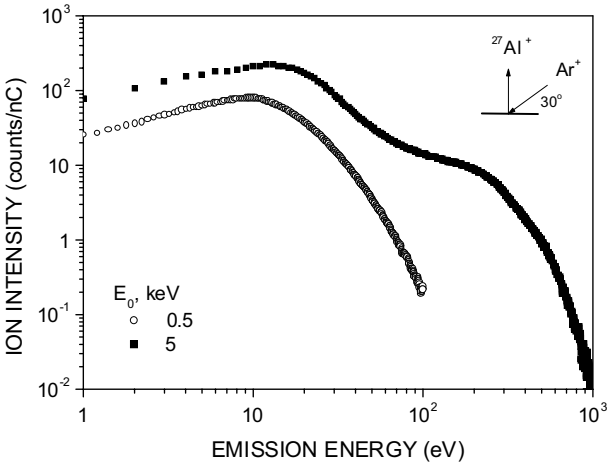

(b)

Fig. 1. Experimental kinetic energy distributions of Al$^+$ secondary ions sputtered under steady-state conditions from a polycrystalline Al sample by Ne$^+$ (a) and Ar$^+$ (b) projectiles with 0.5 keV and 5 keV bombarding energies.

Simulated kinetic energy distributions of Al neutral atoms sputtered from pure aluminium under Ne$^+$ and Ar$^+$ bombardment are shown in Fig. 2. The value of the surface-binding energy, U, is an important input parameter in our simulations. For pure aluminium, we take it equal to the standard atomization energy $U_{\rm Al}$ = 3.4 eV.[23] Figures 2(a) and 2(b) also show the Thompson distributions given by Eq. (5) with the normalization coefficients A(Ω) listed in Table 1. The graphs in Fig. 2 demonstrate that the numerically simulated distributions and the Thompson ones are different, in particular for low bombardment energies and high emission energies. Similar results were reported elsewhere.[22,25,26,35–39]

Table 1. The main parameters of the experimental EDs and the normalization coefficient A of the Thompson distributions of Al^+ secondary ions produced by 0.5 keV and 5 keV Ne^+ and Ar^+ bombardment of pure aluminium. The low- and high-energy characteristic velocities (ionization parameters) were estimated for the plots shown in Figs. 3.

	Ne^+		Ar^+	
	0.5 keV	5 keV	0.5 keV	5 keV
Most probable energy, E_{mp} (eV)	9	16	10	13
Width, $\Delta E_{0.5}$ (eV)	18	24	17	25
Average energy, E_{avr} (eV)	16	54	17	80
Normalization coefficient, A $\left(\frac{\mathrm{at}\cdot(\mathrm{eV})^{0.6}}{\mathrm{ion}\cdot\mathrm{sr}}\right)$	0.752	2.63	0.754	2.88
Low-energy characteristic velocity, v_{01} (10^6 cm/s)	3.1	3.4	3.5	3.2
High-energy characteristic velocity, v_{02} (10^6 cm/s)	—	5.3	—	8.1

In particular, in Refs. 26 and 35, which introduce our simulation model, the numerical simulation has been shown to fit the experimental energy distributions well, whereas the tail portion of the Thompson formula overestimated the yield in comparison to both experimental and simulated distributions. The difference is explained by the contribution of sputtering anisotropies,[32] which lead to a faster decrease of ED with the emission energy than the Thompson formula predicts. In Ref. 40, a simple criterion has been derived that distinguishes the conditions when the Thompson distribution presents a correct slope and when it becomes inaccurate due to the anisotropies. After,[40] the Thompson distribution is reasonably precise when the particle emission energy E satisfies the condition

$$\sqrt{\frac{E+U}{E_i}} \ll \sqrt{\frac{M_t}{M_i}}\,, \tag{8}$$

where E_i is the bombarding projectile energy, M_i is the projectile mass, and M_t is the target atom mass. For example, in the case of 5 keV Ar^+ and Ne^+ bombardment of pure or oxidized Al, the Thompson formula presents a correct shape of the distributions only when the emission energy of sputtered atoms is less than $\sim$ 20–30 eV and $\sim$ 50–60 eV, respectively. At larger emission energies, the Thompson distribution decreases too slowly. With the normalization procedure applied, this leads to the discrepancy seen in Fig. 2. Accordingly with Eq. (8), the discrepancy increases when the projectile energy decreases.

We extracted the normalized Al^+ ion fractions from the experimental energy distributions of the secondary ions $S(E)$ according to the equation

$$P^+(E)\cdot T = \frac{S(E)}{N(E)\cdot I\cdot \Delta\Omega\cdot \Delta E_a}\,, \tag{9}$$

where $\Delta\Omega$ and ΔE_a are the angle and energy "windows" of the registration system. As mentioned above, their values are ca. 10^{-4} sr and 3.5 eV, respectively.

Figures 3(a) and 3(b) show the values P^+T as functions of the normal component of the reciprocal velocity of the secondary ions in the logarithmic scale (the reciprocal or inverse velocity plots). The velocity is represented by $v_n = \sqrt{2E_k/M_{\mathrm{Al}}}\cos\theta$, where $E_k = E + E_b$ is the corrected emission energy and θ is the emission angle ($\theta = 0°$). The energy E_b, which is added to the kinetic energy measured in the experiments, accounts for the surface potential barrier that ionized particles must overcome when they leave the surface. Currently, the nature and exact value of this barrier are not clear enough. An image charge induced in the solid is one possible source of this barrier.[41] Conventionally, E_b is assumed to be equal to the surface-binding energy U,[15,42] or to the difference between the ionization potential of emitted particle and the work function of the bombarded solid (for positively charged secondary ions).[2,43] In our study, we use the surface-binding energy of pure aluminium U_{Al} for correction of the emission energy scale. In any case, an introduction of E_b as well its

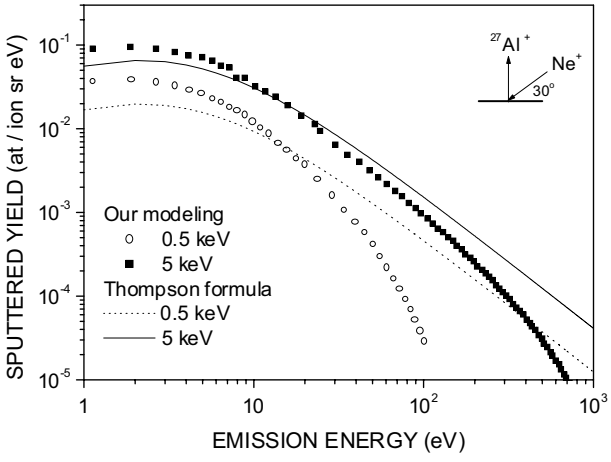

(a)

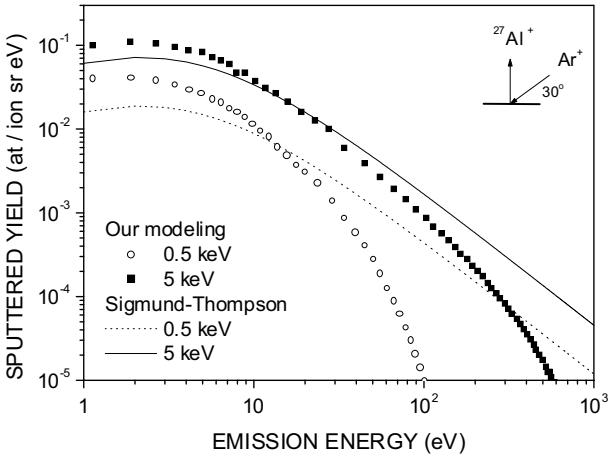

(b)

Fig. 2. Simulated kinetic energy distributions of Al atoms $N(E)$ for 0.5 keV and 5 keV Ne^+ (a) and Ar^+ (b) bombardment of pure Al.

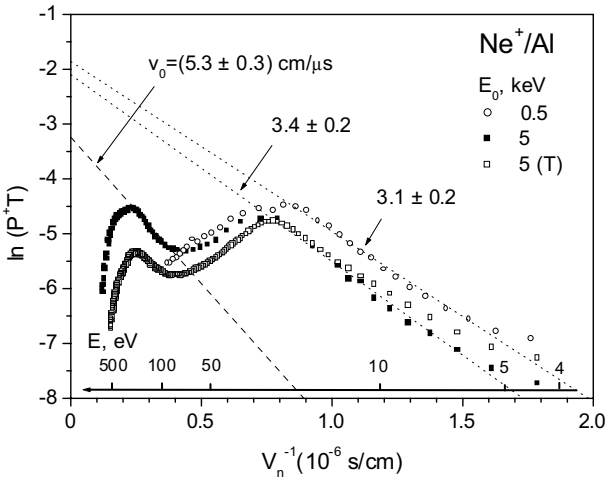

(a)

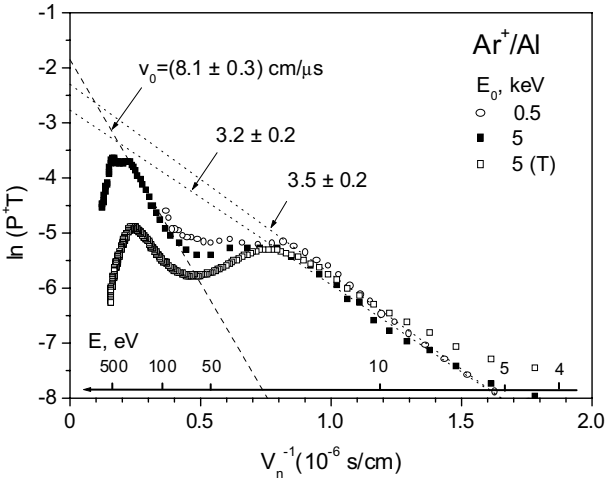

(b)

Fig. 3. Normalized Al^+ ion fraction as a function of the normal component of the reciprocal velocity of the secondary ions under Ne^+ (a) and Ar^+ (b) bombardment with 0.5 keV and 5 keV energies. The data represented by the open squares are obtained employing the Thompson distribution (E_0 = 5 keV). The other graphs are obtained with the distributions $N(E)$ calculated by our original numerical model. The dashed and dotted lines show linear fits of the experimental data with slopes corresponding to the values of the characteristic velocity v_0 (indicated on the panel).

value have no influence on the high-energy part of the reciprocal velocity plots.

The Al^+ reciprocal velocity plots for both Ne^+ and Ar^+ projectiles exhibit a complicated, nonmonotonic shape. We distinguish two velocity (energy) regimes, at low (E_k = 5–25 eV) and high (E_k = 80–280 eV) emission energies, where the experimental curves can be approximated with linear regressions according to Eq. (1). The slopes of the best-fit lines (the dashed and dotted lines in Fig. 3) correspond to the characteristic velocities v_0. Their values are indicated in Fig. 3 and listed in Table 1. In the low-energy regimes, v_{01} is independent of the mass and energy of the projectiles within the limits of the experimental accuracy. In the high-energy regimes, the Al^+ secondary ion yield exhibits a stronger velocity dependency ($v_{02} > v_{01}$), and the value of v_{02} is different for different projectiles. Thus, v_{02} for Ar^+ is larger than that for Ne^+.

The reciprocal velocity plots extracted from our experimental data using the numerical modeling and by the Thompson formula (Fig. 3) look similar in

many respects. The major differences are observed in the very low-energy range (E_k–$U_{Al} = 0$–2 eV), where the "Thompson plots" demonstrate weaker energy dependencies for both type of projectiles. In most of the low-energy regimes, the Thompson plots practically coincide with the other plots and have the same value of v_{01}. Also, both kinds of plots strongly decline in the intermediate-energy regime and demonstrate a less pronounced increase in the high-energy regime. At the same time, the Thompson distribution leads to considerably smaller P^+T values at the emission energies exceeding 25–30 eV in accordance with the criterion given by Eq. (8).

5. Discussion

In this work, we report the reciprocal velocity plots for Al^+ secondary ions. The initial data were measured under well defined experimental conditions, in accordance with the recommendations formulated in Ref. 2. We are unaware of other publications where similar dependencies for the Al^+ ionization probability are obtained in such wide emission energy regimes and complemented with numerical simulation of the energy distributions of sputtered neutrals. Below, we discuss the important features of our velocity plots shown in Fig. 3, and try to clarify, as far as possible, the origins of these features.

For the low-energy linear portion, the characteristic velocity is independent of the mass and energy of the projectiles, which agrees with the tunneling and bond-breaking ionization models.[1,5–7] This means that the effect of the electronic subsystem excitation in the impact region of the surface, recently reported for Si^+ secondary ions produced by atomic and molecular projectiles,[4] is insignificant in the case of aluminium under our bombardment conditions. The velocity plots reach the maximum near $E_k \sim 25$–30 eV, and next, in the intermediate energy regime ($E_k \sim 30$–70 eV), they exhibit the decrease in P^+T values with the increase in the emission energy. A similar peak in the velocity dependence of the ionization probability was observed for different positive secondary ions, including Al^+, in Refs. 20 and 44. It is very likely that ion formation in this energy regime involves more than one channel of electron transitions between the conduction band of solid and electronic states (ground or excited) of emitted particles. As shown in Refs. 44–46, such an interplay of different charge exchange processes can cause peak(s) in the reciprocal velocity plots.

The most interesting, albeit controversial point of our study, is the high-energy linear portion of the velocity plots, which is described by characteristic velocities different from those estimated for the low-energy range. Similar high-energy linear portion was observed by van der Heide[14,15] for negative secondary ions emitted from pure metals under Cs^+, O^- and Ar^+ bombardment. In contract to our measurements, the ions were extracted into a mass–energy analyzer by accelerating electric field. van der Heide suggested that resonance electron transfer processes are responsible for the high-energy linear portion, whereas an Auger-like ionization mechanism prevails in a low-emission energy regime. However, he did not consider the influence of projectile mass on the characteristic velocity, particularly in the high-energy regime.

Both the intermediate and the high-energy regimes of the velocity plots obtained in our work have an important feature to be dependent on the mass of the projectiles. This cannot be explained solely in the framework of the well established ionization models based on Eq. (1). Note that the ratio of the high-energy characteristic velocities $v_{02}(Ar^+)/v_{02}(Ne^+)$ is approximately 1.5 ± 0.1, which is close to the value $\sqrt{M_{Ar}/M_{Ne}}$. This indicates that ballistic transfer of momentum might be involved in the process of formation of the high-energy part of the secondary ion energy distributions. If this is the case, the difference between the characteristic velocities for Ne^+ and Ar^+ projectiles is caused by the difference in kinetic energy transfer from the projectiles to the Al atoms to be emitted directly or by primary recoils knockout. This conclusion is in agreement with our recent results for $A^{III}B^{V}$ compound semiconductors,[30] in which the high-energy tail of secondary ion distributions depend both on the mass of the bombarding ions and on the mass of the second component of the compounds. However, specific details are unclear at the present stage. Several tentative concepts suggest explanations for such an impact:

(i) The numerical model that we use to define the energy distributions of neutral atoms $N(E)$ might be underestimating the contribution from primary and

low-generation secondary recoils so that our velocity plots have distortions in the high-energy region, including the peak on the edge of this regime. Thus, Goehlich *et al.*[39] have observed a maximum in the high-energy portion of the EDs of neutral Al atoms sputtered by Xe^+ ions from pure aluminium, which was confirmed by Monte Carlo TRIM.SP simulations. Should our distributions $N(E)$ have a similar maximum, the resulting velocity plots would be different and perhaps projectile-independent. However, such a maximum was obtained in Ref. 39 only for low-energy (0.5 keV), obliquely incident projectiles, and large oblique angles of sputtered atoms emission. Our trial simulations with the code SRIM[47] did not reveal any high-energy humps in the $N(E)$ function for the relevant bombardment conditions in agreement with our simulation model,[26] although a thorough experimental investigation of the energy distributions of neutral sputtered atoms $N(E)$ is required for definitive conclusions.

(ii) Another explanation can also be suggested. Along with groundstate Al atoms, excited metastable particles might be expected to contribute to the sputtered flux. The energy distributions of the metastable atoms should have a larger contribution from fast particles than the distributions of the groundstate atoms.[48] The secondary ions that originate from the excited sputter population can affect the reciprocal velocity plots, which become dependent on the cascade ballistics. The numerical procedure that we use to obtain the distributions $N(E)$ is accurate for the groundstate population but does not account for the specifics of metastable recoils, from which originate the ballistic sensitivity of the reciprocal velocity plots. Again, experimental investigation is required to verify this hypothesis.

(iii) One more mechanism should be addressed. Recently, Goehlich[22] has observed a high-energy hump in the Thompson type energy distributions of neutral tantalum and tungsten atoms sputtered by 6 keV Ar^+ projectiles from oxygen-covered surfaces. He suggested that the fast metal atoms are generated from the sputtered oxide molecules after their dissociation. The maximum kinetic energy a molecule could receive in a collision without dissociating depends on its binding energy and the ratio of the metal atomic mass to the atomic oxygen mass.[49] Thus, for heavy Ta and W atoms, such energy can reach 90–100 eV, which is enough to form the observed high-energy maximums. However, in the case of light Al atoms, our estimate gives the high-energy cutoff at approximately 30–40 eV, so that such a mechanism appears to be improbable to result in the high-energy features of our plots.

The discussion above demonstrates that the origin of some features in the velocity plots might be more complicated than is currently believed. We leave for the future the ultimate conclusions on the nature of the features that we observe. For now, we would like to comment on the methodical side of our work. Our work demonstrates that both the approach used to obtain the experimental distributions of emitted ions as well as the way to define the distribution $N(E)$ for normalization are critical for the shape of the reciprocal velocity plots and consequently, for their interpretations in terms of underlying physical phenomena. The critical role of the analyzing method has been discussed elsewhere.[2,17,29] Our results confirm that reliable velocity plot measurements, particularly for samples studied under differing bombarding conditions, require analyzers with a small (and constant) angular acceptance and without extracting electric fields. Otherwise, the experimental EDs should be corrected[14,15,50] since the collection efficiency for the ion extraction as well as the energy and the incident angle of projectiles vary during sample potential scans. Such a correction (or reconstruction) is not completely justified and may cause an uncertainty in the shape and intensity of the EDs (for details, see Refs. 2 and 17). At the same time, the basic trends in the velocity (energy) dependence of the secondary ion formation can be qualitatively investigated in the presence of the extraction electric fields.

With regards to the way to define the distribution of neutral sputtered atoms $N(E)$, from our results it follows that kinetic models of sputtering and the normalized Thompson distribution lead to similar shapes of the velocity plots. Thus, the Thompson distribution can be employed for fast, qualitative evaluation of the velocity plots. Also, the normalized Thompson distribution can be used for quantitative evaluation for low emission energies accordingly to the criterion (8), whereas use of the Thompson distribution leads to distortions of the velocity plots for the emission energies that do not satisfy condition (8).

6. Summary

We have examined an advanced approach to characterize the velocity dependencies of Al^+ secondary ion emission produced by 0.5 keV and 5 keV Ne^+ and Ar^+ bombardment of aluminium. We obtained the reciprocal velocity plots from experimental EDs measured over 1–1000 eV of the emission energy without applying electric fields to extract the ions into the mass–energy analyzer. Kinetic simulations by an original computer code as well as the normalized Thompson formula were employed to determine the energy distributions of sputtered neutrals that were used to extract the velocity dependencies of the ionization probability.

The velocity plots of the ionization probability that we observed are nonmonotonic, with peaks and linear portions. The linear portions are rather well approximated by exponential dependencies of the type of the Hagstrum's ansatz[8] with two different values of the characteristic velocity (ionization parameter). For low emission energy (E_k = 5–25 eV), the characteristic velocity is found to be independent of the mass and energy of the projectiles as predicted by the tunneling and bond-breaking ionization models. For the high-energy regimes (E_k = 80–280 eV), the characteristic velocity is larger than that estimated for the low-energy range. Moreover, the high-energy ionization parameter, estimated for Ar^+ projectiles, is larger than that obtained for Ne^+ projectiles.

At present, the genesis of the high-energy features of the reciprocal velocity plots is still not entirely clear. The projectile dependence of the plots indicates that ballistic transfer of momentum under ion bombardment might be contributing. An unanswered question in our work, and the one that is worth further investigation, is whether the projectile dependence of the high-energy portion of the velocity plots is a distortion resulting from an underestimated contribution of fast recoils in the kinetic model of sputtering or a result from a ballistic-dependent mechanism of high-energy secondary ion formation.

References

1. R. Behrisch and K. Wittmaack (eds.), *Sputtering by Particle Bombardment III: Characteristics of Sputtered Particles, Technical Applications* (Springer, Berlin, 1991), p. 91.
2. K. Wittmaack, *Surf. Sci.* **429** (1999) p. 84.
3. M. A. Karolewski and R. G. Cavell, *Surf. Sci.* **480** (2001) p. 47.
4. S. F. Belykh, V. V. Palitsin, A. Adriaens and F. Adams, *Phys. Rev.* **B66** (2002) p. 195309.
5. J. K. Nørskov and B. I. Lundqvist, *Phys. Rev.* **B19** (1979) p. 5661.
6. R. Braco and D. M. Newns, *Surf. Sci.* **108** (1981) p. 253.
7. D. V. Klushin, M. Yu. Gusev, S. A. Lysenko and I. F. Urazgil'din, *Phys. Rev.* **B54** (1996) p. 7062.
8. H. D. Hagstrum, *Phys. Rev.* **96** (1954) p. 336.
9. Z. Šroubek, *Phys. Rev.* **B25** (1982) p. 6046.
10. V. I. Veksler, *Vacuum* **72** (2004) p. 277.
11. M. J. Vasile, *Phys. Rev.* **B29** (1984) p. 3785.
12. R. F. Garrett, R. J. McDonald and D. J. O'Connor, *Surf. Sci.* **138** (1984) p. 432.
13. I. F. Urazgil'din, *Nucl. Instrum. Methods* **B78** (1993) p. 271.
14. P. A. W. van der Heide, *Surf. Sci.* **302** (1994) p. L312.
15. P. A. W. van der Heide, *Surf. Sci.* **341** (1995) p. 150.
16. S. F. Belykh, I. A. Wojciechowski, V. V. Palitsin, A. V. Zinoviev, A. Adriaens and F. Adams, *Surf. Sci.* **488** (2001) p. 141.
17. K. Wittmaack, *Surf. Sci.* **453** (2000) p. L332.
18. P. A. W. van der Heide, *Surf. Sci.* **453** (2000) p. L328.
19. A. Wucher and H. Oechsner, *Surf. Sci.* **199** (1988) p. 567.
20. B. N. Makarenko, A. B. Popov, A. A. Shaporenko and A. P. Shergin, *Radiat. Eff. Def. Solids* **113** (1990) p. 263.
21. S. R. Coon, W. F. Calaway, M. J. Pellin, G. A. Curlec and J. M. White, *Nucl. Instrum. Methods* **B82** (1993) p. 329.
22. A. Goehlich, *Appl. Phys.* **A72** (2001) p. 523.
23. W. Eckstein, *Computer Simulation of Ion-Solid Interactions* (Springer, Berlin, 1991).
24. M. W. Thompson, *Philos. Mag.* **18** (1968) p. 377.
25. J. Dembowski, H. Oechsner, Y. Yamamura and H. M. Urbassek, *Nucl. Instrum. Methods* **B18** (1987) p. 464.
26. M. Stepanova and S. K. Dew, *J. Appl. Phys.* **92** (2002) p. 1699.
27. A. Tolstogouzov, S. Daolio and C. Pagura, *Surf. Sci.* **441** (1999) p. 213.
28. A. Tolstogouzov, S. Daolio and C. Pagura, *Nucl. Instrum. Methods* **B183** (2001) p. 116.
29. A. Tolstogouzov, S. Daolio, C. Pagura and C. L. Greenwood, *Int. J. Mass Spectrom.* **214** (2002) p. 327.
30. A. Tolstogouzov, S. Daolio, C. Pagura, C. L.

Greenwood, D. S. Karpuzov and N. S. McIntyre, *Nucl. Instrum. Methods* **B203** (2003) p. 198.
31. A. Adriaens and F. Adams, *Int. J. Mass Spectrom. Ion Phys.* **108** (1991) p. 41.
32. P. Sigmund, *Phys. Rev.* **184** (1969) p. 383.
33. R. Behrisch (ed.), *Sputtering by Particle Bombardment I* (Springer, Berlin, 1981), p. 9.
34. M. G. Stepanova, *Nucl. Instrum. Methods* **B103** (1995) p. 33.
35. M. Stepanova and S. K. Dew, *J. Vac. Sci. Technol.* **A19** (2001) p. 2805.
36. R. Behrisch and K. Wittmaack (eds.), *Sputtering by Particle Bombardment III: Characteristics of Sputtered Particles, Technical Applications* (Springer, Berlin, 1991), p. 15.
37. L. Wang, R. M. Nor and W. G. Graham, *J. Phys.* **D30** (1997) p. 2379.
38. T. Mousel, W. Eckstein and H. Gnaser, *Nucl. Instrum. Methods* **B152** (1999) p. 36.
39. A. Goehlich, D. Gillmann and H. F. Döbele, *Nucl. Instrum. Methods* **B179** (2001) p. 351.
40. M. Stepanova and S. K. Dew, *Nucl. Instrum. Methods* **B215** (2004) p. 357.
41. B. J. Garrison, *Surf. Sci.* **167** (1986) p. L225.
42. M. J. Vasile, *Nucl. Instrum. Methods* **B40/41** (1989) p. 282.
43. H. Gnaser, *Radiat. Eff. Def. Solids* **109** (1989) p. 265.
44. A. B. Popov, B. N. Makarenko and A. P. Shergin, *Izvestiya RAN, Ser. Fizicheskaya* **58** (1994) (in Russian) p. 47.
45. Z. Šroubek, *Physica Scripta* **T6** (1983) p. 24.
46. B. J. Garrison, D. M. Diebold, J.-H. Lin and Z. Šroubek, *Surf. Sci.* **124** (1983) p. 461.
47. *http://www.srim.org/*
48. E. Dullni, *Appl. Phys.* **A38** (1985) p. 131.
49. H. M. Urbassek, *Nucl. Instrum. Methods* **B18** (1987) p. 587.
50. D. S. Karpuzov and N. S. McIntire, *Nucl. Instrum. Methods* **B187** (2002) p. 311.